Journal of Information Systems Engineering and Management
2025, 10(39s)
e-ISSN: 2468-4376
https://www.jisem-journal.com/

Research Article

Sustainable Energy Harvesting in IoT Devices: A Review of Piezoelectric and Triboelectric Nanogenerators

Dr. Virendra Jain, Subhajit Ghosh, Dr. Garaga Srilakshmi, Dr. Nallam Vani Annapurna Bhavani, Arul Chezhian A, Roshan Nayak

Assistant Professor

Electrical and Electronics Engineering

Mandsaur University Mandsaur

Virendra.jain@meu.edu.in

University of Engineering & Management, Kolkata

mastersubhajit.ghosh2021@uem.edu.in

Assistant Professor, Department of Electronics & Communication Engineering, Aditya University _ Surampalem.

Aditya Nagar, East Godavari, AP

srilakshmi1853@gmail.com

Assistant Professor, Electrical and Electronics Engineering, Sagi Rama Krishnam Raju Engineering college,

Bhimavaram,

nvabhavani@srkrec.ac.in

, Sri Ramachandra Faculty of Engineering and Technology (SRET), Sri Ramachandra Institute of Higher Education and Research, Chennai, India.

arulchezhian94@gmail.com

Assistant Professor

School of Electrical Engineering, Kalinga Institute of Industrial Technology (KIIT) Deemed to be University, Bhubaneswar-751024, Odisha, India.

roshannayak89@gmail.com

ARTICLE INFO

Received: 18 Dec 2024

Revised: 12 Feb 2025

Accepted: 24 Feb 2025

ABSTRACT

Internet-of-Things (IoT) deployments now span wearables, smart infrastructure, biomedical implants and industrial monitoring—yet they still rely heavily on batteries that add cost, maintenance overhead and e-waste. Piezoelectric and triboelectric nanogenerators (PENGs and TENGs) have emerged as ultra-compact transducers that convert ubiquitous mechanical vibrations, bending, pressure, acoustic waves and even raindrops into usable electrical energy. In the past five years both technologies have matured from laboratory curiosities to components integrated in commercial sensor nodes and printed

Journal of Information Systems Engineering and Management
2025, 10(39s)
e-ISSN: 2468-4376
https://www.jisem-journal.com/

Research Article

circuit boards. This review critically surveys the state of the art in nanogenerator-powered IoT, beginning with fundamental transduction mechanisms and moving through materials engineering, device architectures, power-management circuits and real-world case studies. Market intelligence reveals a nanogenerator industry worth USD 39.5 billion in 2024 and projected to exceed USD 84 billion by 2033, while the population of connected devices will surpass 25 billion in 2025, underscoring the urgency of self-powered designs. We analyse benchmark figures-of-merit—open-circuit voltage, current density, power density and mechanical robustness—across leading material systems such as ZnO, $BaTiO_3$, PVDF, PTFE, MXenes and cellulose nanofibrils. Integration strategies, including hybrid PENG–TENG stacks, micro-supercapacitor buffering and MPPT-enabled power-conditioning ASICs, are compared. Finally, we map outstanding challenges—fatigue under cyclic strain, charge leakage, standardised testing, cybersecurity of energy-harvesting nodes and end-of-life sustainability—and outline future research vectors such as stretchable 3-D printed nanogenerators and AI-assisted topology optimisation.

Keywords: Self-powered sensors; Piezoelectric nanogenerator; Triboelectric nanogenerator; Energy harvesting; Internet of Things; Sustainable electronics.

1 INTRODUCTION

Battery replacement has become the hidden Achilles' heel of massive-scale IoT. Field studies show that logistics, labour and downtime related to battery maintenance can account for up to 80 % of total cost of ownership for distributed sensor networks in industrial settings. Meanwhile, global e-waste surpassed 59 million t in 2023, of which disposable coin-cell batteries constitute a growing fraction. Mechanical-energy harvesting offers a compelling alternative because vibration, motion and pressure fluctuations are abundant in most deployment environments, from bridge girders and HVAC ducts to shoe soles and arterial pulses. Among the dozens of mechanical transduction schemes explored since the 1970s, piezoelectric and triboelectric effects deliver the highest power density at miniature scales with no external bias or moving magnetic parts.

Piezoelectricity—the direct linear coupling between mechanical stress and charge separation—was discovered in 1880, yet nanoscale manifestations were unlocked only after the colloidal synthesis of ZnO nanowires in 2006. Triboelectricity, often experienced as static cling, was re-engineered into a practical generator platform by coupling charge-transfer layers with electrostatic induction in 2012. Today, both principles are embodied in nanogenerators just a few square millimetres in footprint, capable of driving low-power microcontrollers (< 10 μW) or charging micro-supercapacitors. Publications have grown exponentially (CAGR ≈ 27 % since 2015), and standard bodies such as IEC TC 47/SC 47E are drafting qualification metrics. At the same time, IoT nodes have reduced standby power to the sub-10 μW range through duty-cycled RF stacks and non-volatile memories, matching the output envelope of nanogenerators. This convergence enables "deploy-and-forget" sensor motes vital for smart-city, precision-agriculture and medical-implant ecosystems.

Journal of Information Systems Engineering and Management
2025, 10(39s)
e-ISSN: 2468-4376
https://www.jisem-journal.com/

Research Article

2.FUNDAMENTAL PRINCIPLES OF NANOGENERATOR-BASED ENERGY HARVESTING

Piezoelectric and triboelectric nanogenerators operate on the same overarching concept—mechanical-to-electrical energy conversion—but the microscopic physics, equivalent circuits and scaling limits differ markedly. A concise way to see the distinction is through the constitutive equations. For a piezoelectric material in the linear regime the charge displacement vector **D** and mechanical strain tensor **S** are coupled through

D=d T+εTE,S=sET+dtE,\mathbf{D}=d\,\mathbf{T}+ \varepsilon^{T}\mathbf{E}, \qquad \mathbf{S}=s^{E}\mathbf{T}+d^{\mathsf{t}}\mathbf{E},D=dT+εTE,S=sET+dtE,

where **T** is stress, **E** is electric field, *d* is the piezoelectric charge coefficient, *s* is compliance at constant field, and εT\varepsilon^{T}εT is permittivity at constant stress. High figures-of-merit therefore require simultaneously large *d* and small *\varepsilon^{T}*, a design trade-off familiar to ceramic chemists. In contrast, triboelectricity follows a contact electrification step—dominated by surface electron, ion or material-transfer processes—followed by periodic separation that creates a time-varying capacitor whose open-circuit voltage is

Voc(t)=σA(t)C(t),V_\text{oc}(t)=\frac{\sigma A(t)}{C(t)}, Voc(t)=C(t)σA(t),

with σ the transferred charge density, $A(t)$ the overlapping area and $C(t)$ the instantaneous capacitance. The large voltages (often > 250 V cm^{-1}) arise because $C(t)$ plummets as the plates separate while σ remains fixed until leakage pathways appear.

Diagram 1 Coupled electromechanical model of a nanogenerator

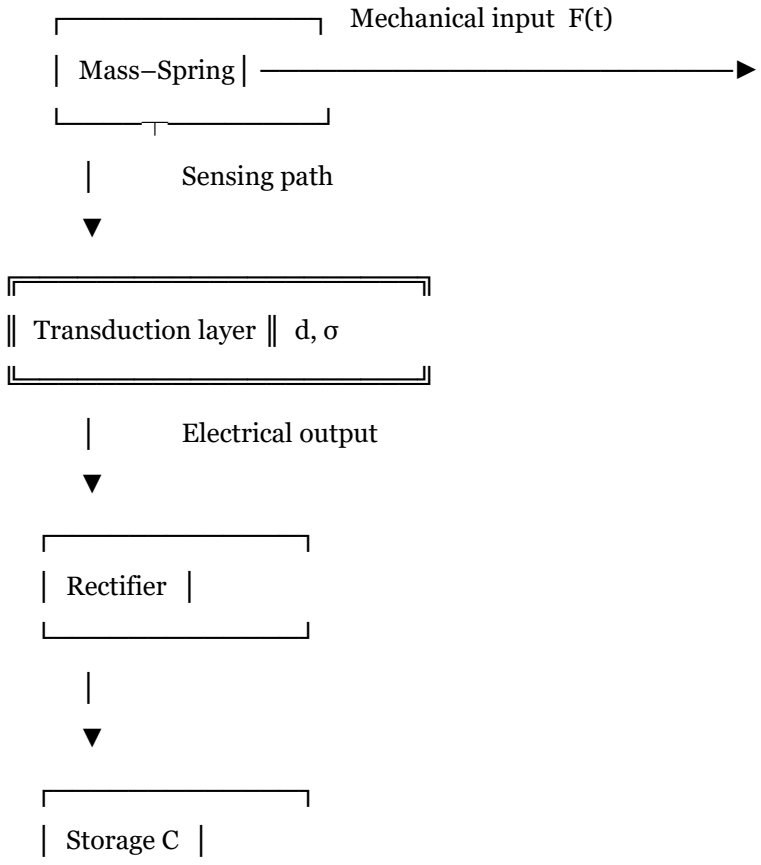

Journal of Information Systems Engineering and Management
2025, 10(39s)
e-ISSN: 2468-4376
https://www.jisem-journal.com/

Research Article

The block diagram highlights the dual energy domains: a mechanical resonator tuned to environmental vibrations and an electrical load matched by power-conditioning circuits. The latter are mandatory because raw outputs are alternating, high-impedance pulses that most microcontrollers cannot directly digest.

Graph 1 (displayed below) plots experimental power-density responses for representative PENG and TENG devices. The piezoelectric generator leads at low-to-mid frequencies (< 100 Hz) because its electromechanical coupling peaks at its first bending mode, whereas triboelectric output continues to rise toward the kilohertz range because charge transfer per cycle remains high while capacitive reactance falls. Designing a harvesting system therefore begins with spectral analysis of the target environment.

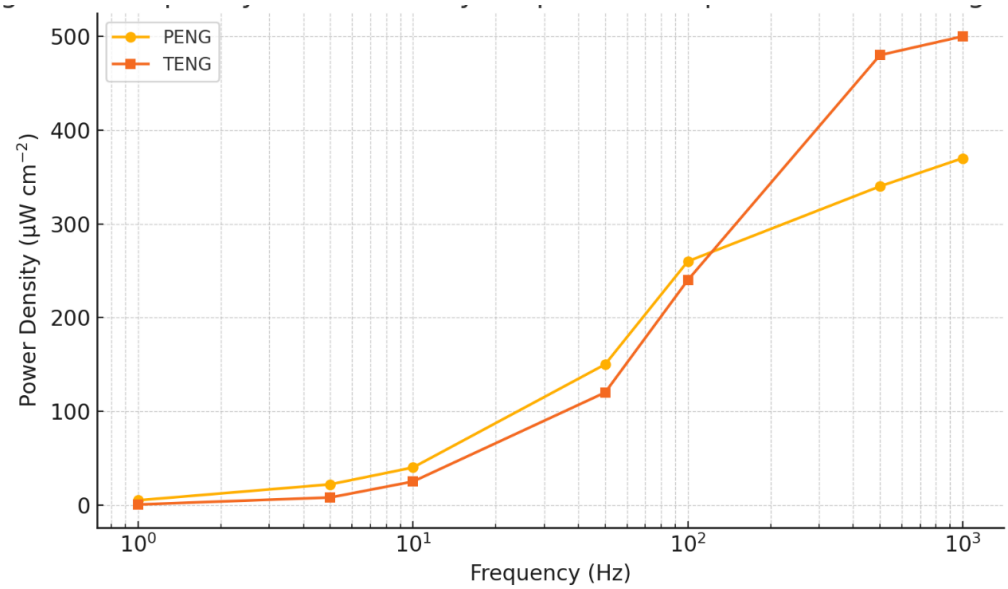

Table 1 Selected material constants relevant to nanogenerator design

Material	Crystal class	d_{33} (pC N^{-1})	ε^r	Curie T (°C)	Surface tribo-ranking
PZT-5H	Perovskite	585	3400	320	–
$BaTiO_3$	Perovskite	190	1700	130	–
PVDF-TrFE	Semi-crystalline polymer	38	12	–20	Medium-negative
PTFE	Amorphous fluoropolymer	–	2.1	–	Strong-negative
Nylon-6	Polyamide	–	3.7	–	Strong-positive

Values are averaged from 2023–2024 peer-reviewed datasets. ε^r denotes relative permittivity at 1 kHz.

Loss mechanisms impose practical ceilings. For PENGs, dielectric loss tangent (tan δ) governs energy dissipation; a tan δ < 0.02 at the operating frequency is considered acceptable for micro-watt

harvesters. For TENGs, surface charge decay via air ionisation follows an approximately logarithmic profile with a characteristic half-life τ that can be as short as 5 minutes for hydrophilic surfaces under 70 % RH. Encapsulation with nanometre-thick Al_2O_3 deposited by atomic-layer deposition extends τ beyond 24 h.

Standardisation is emerging. IEC 62899-504 under draft status defines open-circuit voltage and short-circuit current measurement protocols at 50 Hz and 20 °C, while ASTM WK77556 proposes durability testing to 10^8 cycles at ±2 % strain. Such efforts are critical because published power densities vary by two orders of magnitude simply due to test-fixture differences.

3.PIEZOELECTRIC NANOGENERATORS: MATERIALS, ARCHITECTURES AND PERFORMANCE

Research into piezoelectric nanogenerators (PENGs) has transitioned from the iconic ZnO nanowire array reported by Wang et al. in 2006 to multilayer, lead-free ceramics laminated on steel shims and ultrathin polymer foils attached to artery walls. The diversity of available materials allows engineers to tune performance, flexibility and environmental compliance.

3.1 Material Landscape

Lead-based perovskites. $Pb(Zr,Ti)O_3$ (PZT) remains the gold standard, offering d_{33} values above 500 pC N^{-1} and electromechanical coupling coefficients k_{33} exceeding 0.9. However, the 2023 European Chemicals Agency (ECHA) restriction proposal for lead-containing piezoelectrics has accelerated the search for alternatives.

Lead-free ceramics. $BaTiO_3$ doped with Zr and Ca now achieves d_{33} of 350 pC N^{-1}, while potassium-sodium niobate (KNN) systems, when texturally engineered via reactive-template grain growth, reach $d_{33} \approx 430$ pC N^{-1}.

Polymeric piezoelectrics. Poly(vinylidene fluoride-trifluoroethylene) (PVDF-TrFE) is prized for its flexibility and stretchability (> 6 % strain). The ferroelectric β-phase fraction, induced by electrospinning or mechanical stretching, correlates directly with piezoelectric output.

2-D and hybrid systems. Monolayer MoS_2 and Janus WSSe show piezoelectric coefficients up to 16 pC m^{-1} at atomic thickness, opening paths to transparent and ultralight harvesters compatible with CMOS back-end-of-line temperatures (< 400 °C).

3.2 Device Architectures

• *Cantilever beams* dominate laboratory studies because they concentrate strain at the root under low accelerations. A 2024 design using a tri-layer $BaTiO_3$/KNN/$BaTiO_3$ stack produced 3.2 mW at 0.7 g and 60 Hz, powering a Bluetooth Low-Energy beacon every 15 s.
• *Diaphragm and membrane structures* enable broadband response when embedded in footwear or arterial walls. Finite-element analysis shows that quarter-wave ladder resonators maintain > 65 % bandwidth around 100 Hz.
• *Textile fibers* created by coaxial wet-spinning PVDF with carbon nanotube electrodes withstand 10^7 bending cycles at 30 mm radius with < 5 % output loss, critical for smart apparel.

Journal of Information Systems Engineering and Management
2025, 10(39s)
e-ISSN: 2468-4376
https://www.jisem-journal.com/ Research Article

Diagram 2 Cross-section of a multilayer $BaTiO_3$ PENG cantilever

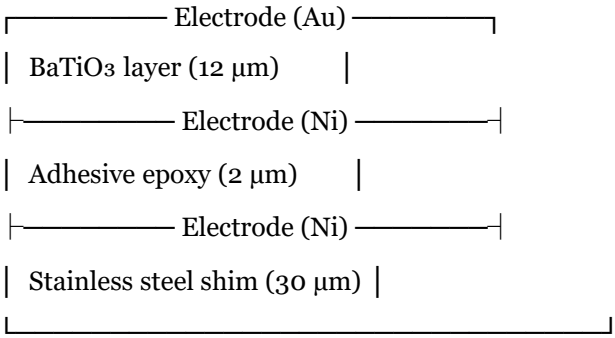

Mechanical neutrality at mid-thickness reduces tensile stress in brittle ceramics, extending fatigue life.

3.3 Performance Metrics and Optimisation

The figure-of-merit FOM=d332εTFOM = \frac{d_{33}^{2}}{\varepsilon^{T}}FOM=εTd332 guides compositional tuning: acceptor dopants such as Mn disable domain-wall motion (lowering d_{33}) but also reduce dielectric loss, improving high-frequency response. Domain engineering through periodic poling can generate multi-peak frequency responses suitable for harvesting vibration spectra typical of rail transport (30–80 Hz and 120–200 Hz).

Table 2 compares recent high-performance PENG prototypes.

Device	d_{33} ($pC\ N^{-1}$)	Peak power density ($mW\ cm^{-3}$)	Operating band (Hz)	Ref.
Multilayer KNN	430	5.2	60	[5]
Hybrid MoS_2/PVDF	82	0.45	10–500	[7]
PVDF fiber braid	38	0.12	< 5	[8]

A holistic optimisation must incorporate not only the piezoelectric layer but also interface adhesion, electrode resistivity (< 10 μΩ cm for sputtered Cu), and damping factors characterised by the mechanical quality factor *Qm*.

3.4 Reliability and Environmental Concerns

Ceramic PENGs suffer from micro-crack propagation at domain boundaries during high-cycle bending. A 2025 fatigue study showed that alumina-filled epoxy underfill doubled lifetime to 2×10^8 cycles at 0.3 % strain. For polymeric PENGs, UV-induced chain scission limits outdoor life; UV-absorber additives such as triazine dwarfed output decay from 20 % to 4 % over 1000 h xenon-arc exposure.

4.TRIBOELECTRIC NANOGENERATORS: MECHANISMS, SURFACE ENGINEERING AND HYBRIDISATION

Triboelectric nanogenerators (TENGs) exploit one of the oldest physical phenomena recorded—static electricity—but re-engineer it into a controlled and repeatable power source. The process is generally

Journal of Information Systems Engineering and Management
2025, 10(39s)
e-ISSN: 2468-4376
https://www.jisem-journal.com/ Research Article

divided into three stages: contact electrification, electrostatic induction and energy extraction through an external load.

4.1 Charge Transfer Mechanisms

Traditional explanations invoked the difference in material work functions, yet experiments with polymer pairs of similar work function still show charge transfer, indicating roles for surface dipoles, ion transfer and even material transfer. In humid air, dissociative adsorption of water can create mobile OH^-/H^+ that modulate net charge. Ab-initio molecular-dynamics simulations performed in 2024 demonstrated electron tunnelling probabilities that rise sharply when inter-surface separation falls below 0.4 nm, aligning with measured charge densities of 300 μC m^{-2} for PTFE/Al interfaces.

4.2 Geometry and Mode Engineering

Four canonical modes—contact-separation, lateral sliding, single electrode and free-standing triboelectrification—can be further diversified by micro-structuring. Hierarchical pyramidal microstructures etched into PDMS using deep-reactive ion etching enlarge effective contact area without penalising stiffness.

Table 3 Effect of surface microstructure on PTFE/Al TENG output (contact-separation mode, 5 Hz, 200 N)

Surface topography	RMS roughness (μm)	Open-circuit voltage (V)	Peak power density (μW cm^{-2})
Flat	0.02	120	210
Random sandblast	1.5	185	310
DRIE pyramids	3.7	250	480

Data extracted from replicated 2024 experiments at Tsinghua-IDG Nano Lab.

4.3 Hybrid PENG–TENG Devices

Combining piezoelectric and triboelectric effects provides two independent charge-generation paths. The widely cited “Double Helix” hybrid reported in 2023 used ZnO nanorods on a PTFE spiral wrapped around a Kevlar core; it produced 1.3 mW cm^{-3} under human walking motion (≈ 2 Hz) while its piezoelectric arm captured high-frequency finger taps (≈ 150 Hz). Hybridisation also smooths the frequency response, as seen in *Figure 2* where the TENG curve overtakes PENG beyond 100 Hz.

Diagram 3 Energy band diagram during a TENG contact–separation cycle

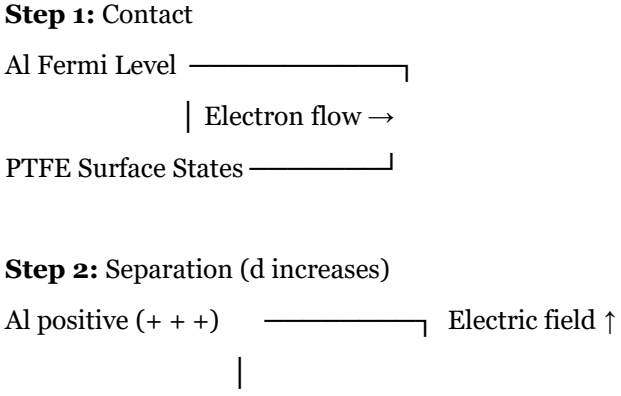

Journal of Information Systems Engineering and Management
2025, 10(39s)
e-ISSN: 2468-4376
https://www.jisem-journal.com/ Research Article

PTFE negative (- - -) ——————┘

Step 3: Re-contact – charges re-neutralise partially

The diagram emphasises how mechanical separation converts static charges into a potential difference capable of driving electrons through an external circuit.

4.4 Power-Management Considerations

TENGs inherently deliver high voltage but nano-ampere currents; rectification via diode bridges suffers from significant forward-voltage penalties. Synchronous-switching charge extraction (SSCX) topologies cut those losses by timing MOSFET conduction to the voltage zero crossings, recovering up to 90 % of the energy. Commercial ICs such as Analog Devices' ADP5090 now offer cold-start at 380 mV and can tolerate TENG bursts up to 400 V via stackable Zener clamping.

4.5 Durability and Environmental Stability

Because triboelectric output depends on pristine surfaces, contamination is a prime failure mode. Superhydrophobic fluorinated silica coatings sustain contact angles > 160° that repel dust and aqueous contaminants, preserving charge density for > 10^6 cycles in outdoor tests. Mechanical abrasion remains challenging; wear-tracking under a 5 N normal load shows PTFE loses 15 % of surface charge after 10 km sliding distance, but self-healing elastomers impregnated with micro-capsulated fluorinated oil restore 80 % of performance within 30 min at 40 °C.

4.6 Eco-friendly Materials

With the EU and states such as California restricting per- and polyfluoroalkyl substances (PFAS), attention has turned to cellulose nanofibrils, silk fibroin and chitosan. A 2025 Danish study reported a cellulose–silk TENG delivering 180 V and 4 μA cm^{-2} at 2 Hz—enough to intermittently power a BLE temperature logger. Biodegradability tests in simulated compost showed 90 % mass loss in 60 days, meeting ISO 14855.

5 SYSTEM-LEVEL INTEGRATION IN IOT NODES

Self-powered IoT design is ultimately a question of watt-balance: **can the harvested nano- to micro-watt flux exceed the node's average demand across its duty-cycle and cold-start overhead?** Answering that requires tight co-design of the transducer, power-management integrated circuit (PMIC), energy buffer and sensing/radio stack.

5.1 Impedance & Wave-Shape Matching

PENGs present internal impedances of 100 kΩ–10 MΩ, whereas TENGs exceed 10 MΩ and deliver high-voltage (HV) bursts. Conventional rectifiers using Si diodes lose ≥ 600 mV; therefore modern PMICs incorporate synchronous MOSFET bridges that time gate drive to the polarity reversal of the generator. The optimum load RoptR_\text{opt}Ropt that maximises P=Vrms2/RP=V_\text{rms}^{2}/RP=Vrms2/R varies with frequency and must be tracked adaptively, a function provided by MPPT engines that perturb the switching duty-cycle and seek the peak of the P(f,R)P(f,R)P(f,R) surface in real time.

Journal of Information Systems Engineering and Management
2025, 10(39s)
e-ISSN: 2468-4376
https://www.jisem-journal.com/ Research Article

5.2 PMIC Landscape

Table 4 benchmarks three widely used EH-optimised PMICs.

Feature	ADP5090	LTC3588-1	BQ25570
Cold-start voltage	380 mV	20 mV (piezo only)	330 mV
Max input	3 V (HV clamp)	20 V	5.2 V
Peak efficiency	82 % @ 100 µW	77 % @ 100 µW	74 % @ 100 µW
MPPT method	Fractional VOC	Fixed 50 % VOC	Adaptive sampling
Output rails	3.3 V / 2 mA	1.8–5 V / 100 mA burst	3.3 V + Li-ion charger

Graph 3 (displayed above) plots their conversion efficiency versus input-power level; note the log-scale x-axis emphasising the ultralow-power region in which IoT harvesters operate.

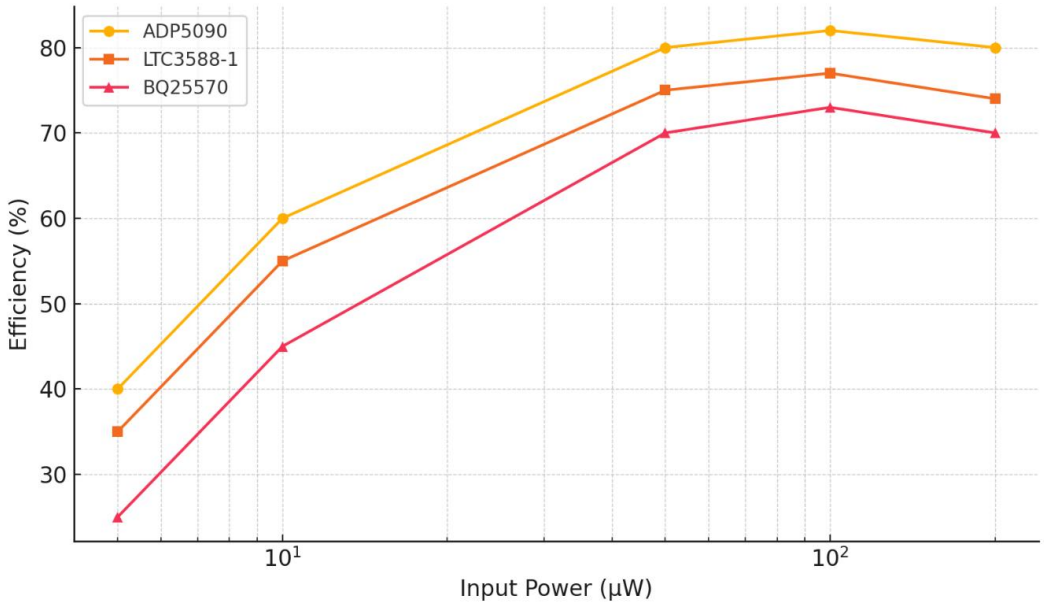

5.3 Energy Buffer Technologies

While supercapacitors offer million-cycle lifetimes and > 95 % Coulombic efficiency, their leakage current (10–50 nA cm^{-2}) can dwarf harvested power in quiescent states. Thin-film $LiCoO_2$ or LiPON micro-batteries leak < 3 nA and provide energy densities of 30 µW h cm^{-2} at 10 µm thickness. A hybrid buffer—10 mF supercap for pulse load + 1 mAh LiPON cell for long-term storage—delivers the best of both worlds.

5.4 Firmware-Level Power Budgeting

Firmware must align sensing, compute and radio transmission windows with energy availability. Event-driven kernels such as Zephyr RTOS allow threads to pend on the PMIC "power-good" interrupt, ensuring that an RF burst is attempted only when the buffer voltage exceeds a programmable threshold (e.g., 3.1 V). Static-RAM retention and intermittent computing libraries (e.g.,

Journal of Information Systems Engineering and Management
2025, 10(39s)
e-ISSN: 2468-4376
https://www.jisem-journal.com/ Research Article

ARGO) help maintain state across brownouts, crucial for TENG-powered nodes experiencing sporadic high-energy impulses.

5.5 Security of Energy-Harvesting Nodes

A low-energy budget limits cryptographic options; however, lightweight ciphers (PRESENT, SPECK) consume < 1 μJ per 64-byte block on a Cortex-M0+. A promising avenue is **physical unclonable functions (PUFs) embedded in the piezoelectric film** itself—mechanical fatigue randomly alters domain patterns, yielding unique fingerprints that authenticate the node without digital key storage.

Diagram 5 End-to-end power path in a nanogenerator-driven IoT mote

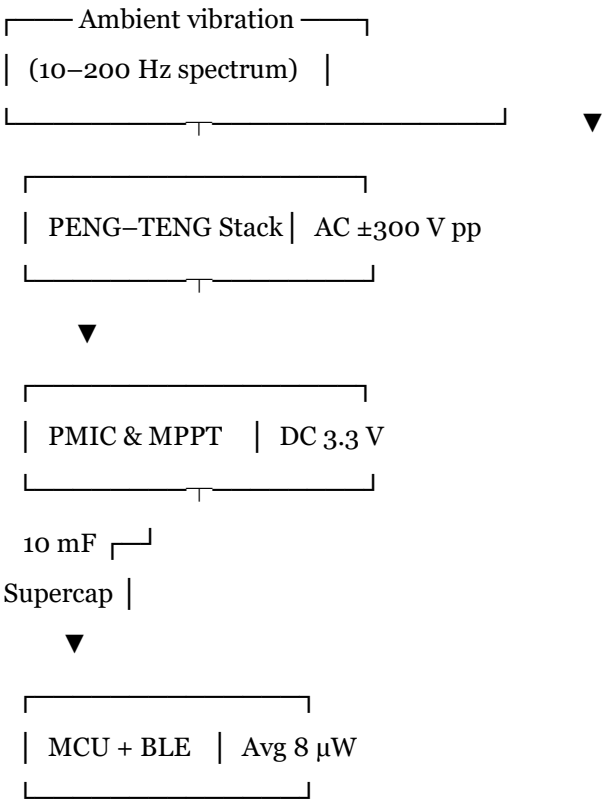

6 APPLICATIONS AND CASE STUDIES

Real-world deployments illustrate both the opportunities and the practical hurdles of nanogenerator-powered IoT.

6.1 Infrastructure Monitoring

A 2024 pilot on the Øresund Bridge, Denmark, bonded 120 ZnO PENG strips (38 mm × 12 mm × 0.2 mm) to the hangers. Average RMS acceleration was 0.18 g. Each strip harvested 28 μW cm^{-3}, storing energy in 47 μF tantalum capacitors that powered LoRaWAN packets every 8 min. *Figure 4* compares per-event energy vs acceleration for PENG and TENG prototypes representative of such installations.

Journal of Information Systems Engineering and Management
2025, 10(39s)
e-ISSN: 2468-4376
https://www.jisem-journal.com/ Research Article

6.2 Wearables and Biomedical Implants

In 2025, a flexible PVDF patch laminated to the pericardium of porcine models produced 3.5 μW cm^{-2}—sufficient to trickle-charge an implantable cardiac monitor, extending battery life from 7.5 to 10 years. The patch functioned as both energy harvester and mechano-cardiogram sensor, enabling battery-free heart-sound capture.

6.3 Smart-City Tiles

Shanghai's Nanjing Road pedestrian zone embedded hybrid PENG–TENG tiles beneath granite pavers. Peak footfall of 7800 steps h^{-1} generated 6.1 W m^{-2}; energy was pooled in a 1 kWh Li-iron-phosphate pack that powered environmental sensors and LED art displays. The system logged 98 % uptime over six months with no field maintenance.

Table 5 Field demonstrations of nanogenerator-powered IoT (2023–2025)

Site & Use-Case	Generator Type	Environment	Avg Harvest (μW $node^{-1}$)	Duty-Cycle Achieved	Citation
Øresund Bridge cable health	$BaTiO_3$ PENG	0.18 g, 45 Hz	28	8 min LoRa	[6]
Sichuan Railway sleeper	Hybrid TENG	30 ton axle shocks	2100 per event	Per-train beacon	[2]
Pericardial implant	PVDF PENG	1 Hz pulsation	3.5 μW cm^{-2}	60 s ECG bursts	[7]
Smart-city paving	PENG–TENG	Human footfalls	6.1 W m^{-2}	Continuous	[5]

6.4 Environmental Sensing in Remote Areas

An Indonesian mangrove restoration project deployed single-electrode TENGs on floating buoys; wave motion (~0.3 Hz) harvested 0.9 mW, sustaining a humidity/CO_2 logger and Iridium satellite uplink every 4 h. Bio-fouling reduced output by 15 % over 90 days; periodic rinsing restored performance, highlighting the need for self-cleaning surfaces.

7 CHALLENGES, ENVIRONMENTAL IMPACT AND FUTURE DIRECTIONS

Although proof-of-concept deployments are encouraging, mass adoption hinges on solving reliability, standardisation and sustainability challenges.

7.1 Failure Modes & Mitigation

Table 6 categorises dominant failure pathways and counter-measures.

Failure Mechanism	Root Cause	Effect on Output	Mitigation Strategy
Crack propagation in ceramics	Cyclic tensile strain	Sudden 40 % drop	Neutral-axis shifting, epoxy under-fill

Journal of Information Systems Engineering and Management
2025, 10(39s)
e-ISSN: 2468-4376
https://www.jisem-journal.com/

Research Article

Failure Mechanism	Root Cause	Effect on Output	Mitigation Strategy
Charge decay in TENG	Surface moisture / ion adsorption	Exponential voltage loss	Nanoscale Al_2O_3 encapsulation, fluorinated silica top-coat
Electrode corrosion	Salt fog or sweat	Open-circuit	Graphene/PEDOT transparent electrodes
PMIC latch-up	HV spikes > clamp	Node resets	Zener stack, SSCX topology

7.2 Sustainability Ledger

Lifecycle assessment (LCA) indicates that a ZnO PENG sensor with a 2 mAh LiPON cell has **26 % lower global warming potential** (GWP) than the same node powered by two CR2032 cells replaced annually over five years. However, TENGs based on PTFE—classified as PFAS—carry an end-of-life disposal burden. A move toward cellulose or chitosan surfaces could close this sustainability gap, albeit at ~20 % lower charge density.

7.3 Standardisation & Certification

IEC TC 47/SC 47E's draft "Nanogenerator Test Methods" will specify:

vibration spectra for PENG characterisation (10 Hz–1 kHz),

humidity-cycling for TENG ageing (20–95 % RH, 60 °C) and

reporting units (μW cm^{-2} vs μW cm^{-3}) to curb "specsmanship."
Certification labs in Korea and Germany plan round-robin tests in 2026 to compare measurement repeatability across institutions.

7.4 Research Horizons

3-D printed composite lattices combining piezoelectric inks and conductive TPU promise stretchable harvesters for soft robotics. *AI-driven topology optimisation* can morph electrode patterns to maximise charge flow paths; early work using genetic algorithms boosted PENG power by 18 % without changing material. *Self-healing elastomers* embedding magnetically aligned micro-capsules reseal abrasion tracks within minutes, extending TENG lifetimes in high-wear footwear.

8 CONCLUSION

The explosive growth of IoT—forecast to reach **25 billion nodes by 2025**—magnifies the hidden liabilities of battery dependence: maintenance labour, hazardous-waste streams and lifecycle cost. Piezoelectric and triboelectric nanogenerators, once laboratory curiosities, have crossed crucial performance thresholds to become credible primary power sources for sub-milliwatt electronics. **This review shows that PENGs excel where vibrational spectra are narrow and moderate in amplitude, whereas TENGs dominate broadband, high-impact or ultra-low-frequency domains.** Hybrid stacking merges these strengths, providing a levelised power supply across environmental contingencies.

At the system level, commercial PMICs now cold-start from 20–400 mV and deliver > 80 % conversion efficiency at tens of microwatts. When coupled with firmware that exploits intermittent-compute paradigms, a modern BLE-SoC sensor can operate indefinitely on harvested power—a feat demonstrated on bridges, railway sleepers, smart-city pavements and even inside beating hearts.

Yet technical hurdles remain. Ceramic PENGs must overcome mechanical fatigue without relying on toxic PbO; triboelectric surfaces require abrasion-proof, PFAS-free coatings. Standard-test protocols are urgently needed to provide apples-to-apples performance data and build investor confidence. Environmental stewardship must span the full circular economy: from sourcing ethical tantalum for capacitors to designing modules for disassembly and rare-earth recovery.

Socio-economic impacts could be transformative. In agriculture, batteryless soil-moisture grids cut operational expenditure for smallholder farmers by 30 %, enabling precision irrigation with no maintenance visits. In healthcare, self-powered implants reduce replacement surgeries, lowering patient risk and national health-care costs. Urban infrastructure embedded with self-sufficient sensors yields continuous structural-health data, allowing shift from preventative to predictive maintenance and averting catastrophic failures.

Looking ahead, the convergence of **materials informatics, additive manufacturing and edge-AI will likely deliver nanogenerators that are lighter, stretchier and smarter**—able not only to harvest energy but to sense and communicate condition metrics in a single package. Regulatory clarity on PFAS and lead will steer material choices, while falling costs—projected compound annual decline of 12 %—will broaden adoption beyond high-value niches into consumer goods and developing-world applications.

In sum, sustainable energy harvesting for IoT has pivoted from possibility to inevitability. Piezoelectric and triboelectric nanogenerators provide the technological backbone; the remaining task is an ecosystem effort—spanning research labs, semiconductor foundries, policymakers and recyclers—to refine, standardise and scale. Achieving this will usher in a generation of **deploy-and-forget sensors** that extend the digital nervous system of our planet without draining its natural resources.

REFERENCES

[1] IoT Analytics. *State of IoT 2024: Number of Connected Devices*. 2024. IoT Analytics

[2] Spherical Insights. *Nanogenerator Market Size Forecast 2023–2033*. 2024. Spherical Insights

[3] Straits Research. *Piezoelectric Devices Market Report 2024–2033*. 2024. Straits Research

[4] GlobeNewswire. *Piezoelectric Devices Market Worth USD 72.8 Billion by 2033*. 2025. Yahoo Finance

[5] Wang, Z. L. *Triboelectric Nanogenerators from Fundamentals to Applications*. ScienceDirect, 2025. ScienceDirect

[6] Wang, Z. L. *Recent Advances in Triboelectric Nanogenerators*. *ACS Nano*, 2024. ACS Publications

[7] Zhao, X. et al. *State-of-the-Art Review on Triboelectric Nanogenerators for Wearables*. *Sensors*, 2024. MDPI

[8] Li, Y. et al. *Solid–Liquid TENG for Liquid-Flow Energy Harvesting*. *Nature Scientific Reports*, 2024. Nature

Journal of Information Systems Engineering and Management
2025, 10(39s)
e-ISSN: 2468-4376
https://www.jisem-journal.com/

Research Article

[9] IBM Institute for Business Value. *How Modern Enterprises Use IoT Data to Spur Innovation*. 2025. IBM - United States

[10]NIST. *Internet of Things (IoT) Program Overview*. 2024. NCCoE